THE JOURNAL OF PHYSICAL CHEMISTRY B

Article

pubs.acs.org/JPCB

Influence of the Molecular Environment on Phosphorylated Amino Acid Models: A Density Functional Theory Study

Maria E. Rudbeck,*[,†] Sten O. Nilsson Lill,[‡] and Andreas Barth*[,†]

[†]Department of Biochemistry and Biophysics, The Arrhenius Laboratories for Natural Sciences, Stockholm University, SE-106 91 Stockholm, Sweden

[‡]Department of Chemistry, University of Gothenburg, SE-412 96 Göteborg, Sweden

Supporting Information

ABSTRACT: A protein environment can affect the structure and charge distribution of substrate molecules. Here, the structure and partial charges were studied for different phosphorylated amino acid models in varying environments using density functional theory. The three systems investigated, acetyl phosphate, methyl phosphate, and *p*-tolyl phosphate are representative models for aspartyl phosphate, serine or threonine phosphate, and tyrosine phosphate, respectively. Combined with the CPCM continuum model, explicit HF and H_2O molecules were added in order to model environmental effects and interactions that may occur in a protein matrix. We show how the different interactions affect the scissile P−O(R) bond and that the elongation can be explained by an anomeric effect. An increasing scissile bond length will result in transfer of negative charge to the leaving group and in a widening of the angle between the terminal oxygens of the phosphate molecule, features that can expose the phosphate group to attacking nucleophiles. Lastly, calculations were performed on the active site of the Ca^{2+}-ATPase E2P intermediate, which provide an example of how a protein environment facilitates the formation of a destabilized ground state.

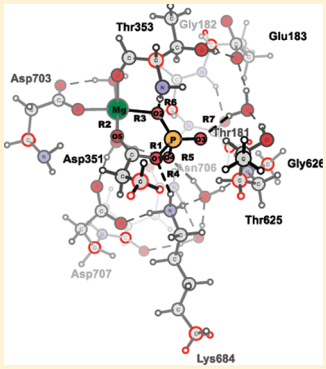

1. INTRODUCTION

Phosphorylation is one of the fundamental regulatory mechanisms in biology. Therefore, phosphate transfer reactions are catalyzed by a large number of enzymes comprising kinases, mutases, and phosphatases. Enzymatic reactions are accelerated up to ~10^{21}-fold compared to the uncatalyzed reactions due to specific interactions between the protein and substrates.[1] These interactions are commonly thought to stabilize the transition states of the reactions but may already in the ground state generate a conformation that resembles the transition state structure.[2,3]

In order to better understand phosphate transfer reactions in different enzymes, studies of small phosphate models are crucial. Even though many studies[4−10] have been performed on phosphoric monoesters, important questions regarding their phosphate transfer reactions are still unanswered. Cheng et al.,[4] using vibrational spectroscopy, and Range et al.,[9] using density functional theory (DFT) calculations, found that the pK_a of the leaving groups correlates with the P−O(R) bond length for a large number of phosphorylated compounds. Earlier, using crystallographic and kinetic data, Jones and Kirby[11] found that both the pK_a and the bond length of the scissile P−O bond correlate with the hydrolysis rate. Thus, the bond length and bond strength of the scissile P−O bond length are crucial parameters in understanding the ease of dephosphorylation.

A chemical model that can help explain the extended bond lengths is negative hyperconjugation, the main contribution to the stereoelectronic effect known as the anomeric effect. Within phosphates, it involves the interaction between the terminal oxygens' *n*-orbitals (donors) and the empty antibonding σ^*-orbital (acceptor) of the bridging P−O bond, producing an extended molecular orbital. Ruben et al.[5,6] have shown that the negative hyperconjugation weakens the bridging P−O bond and thereby contributes to the exothermicity of hydrolysis. DuPré et al.[7] have analyzed the stereoelectronic states of the dimethyl phosphate ion and included a hydrogen-bonding water molecule or a cation, interacting with the terminal oxygens, in order to study the delocalization of the charge from the lone pairs of the terminal oxygens toward the ligand. Their calculations showed that both interactions strengthened the bridging P−O bond. All of the above studies were performed with natural bond orbital (NBO) analysis.[13]

Molecular properties that influence phosphate transfer reactions have mainly been studied by comparison between different phosphorylated molecules. Only a few studies deal with environmental effects. Abell and Kirby[14] found experimentally that the P−O bond cleavage in phosphate monoester dianion reactions was accelerated in media less protic than water, such as DMSO. A similar experimental study was performed by Grzyska et al.[15] with a series of phosphate esters with more basic leaving groups. They found a dehydration-induced weakening of the P−O bond of aryl phosphate esters and a concomitant acceleration of hydrolysis by DMSO in aqueous solution, which is consistent with the work of Abell and Kirby. Methyl phosphate

Received: July 7, 2011
Revised: January 30, 2012
Published: February 4, 2012

and phenyl phosphate hydrolysis, however, is slowed down when increasing the DMSO/water ratio. De Meis and Vianna[16] measured the hydrolysis of acetyl phosphate and ATP in water with different amounts of organic solvent. Also here a decrease in water activity promotes an increase in the rate of the hydrolysis of phosphate compounds in solution. Their work also indicated that these trends can be extrapolated to enzymes involved in energy transduction, i.e., a decrease in water activity within a catalytic site accelerates hydrolysis of the phosphate compound.

That a protein environment affects the structure and charge distribution of substrate groups has been experimentally verified and characterized by, for example, vibrational spectroscopy.[4,17−22] One example is the sarcoplasmic reticulum Ca^{2+}-ATPase,[17] which is a Ca^{2+} pump driven by ATP hydrolysis.[17,23,24] During its reaction cycle, ATP phosphorylates Asp351 and generates two consecutive phosphoenzyme intermediates Ca_2E1P and E2P. One of the intriguing properties of E2P is its rapid hydrolysis in contrast to the slow hydrolysis of the model compound acetyl phosphate in aqueous solution. In this study, we were interested in the specific interactions within the Ca^{2+}-ATPase, in particular those important for the fast hydrolysis. In order to better evaluate the different interactions, we initially studied three phosphorylated compounds, which represent three different phosphorylated amino acids that occur in cells.

Density functional theory (DFT) calculations were performed on acetyl phosphate, methyl phosphate, and *p*-tolyl phosphate, which are representative models for aspartyl phosphate, serine or threonine phosphate, and tyrosine phosphate, respectively (see Figure 1) interacting with either the highly

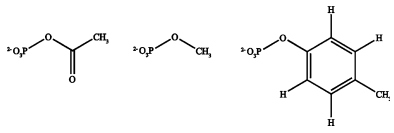

Figure 1. Acetyl phosphate (AcP), methyl phosphate (MP) and *p*-tolyl phosphate (TP).

polar hydrogen fluoride (HF) molecule or H_2O. HF was chosen due its polarity but also to serve as a model for a single hydrogen donor, allowing us to study specific hydrogen−oxygen interactions. With H_2O, it is more difficult to model one specific interaction since it is energetically more favorable to hydrogen bond to two oxygens simultaneously. The effects of the interactions on energy, charge distribution, geometry, and negative hyperconjugation were studied and compared to calculations performed on a model of the active site of E2P.

2. METHODS

2.1. Simple Environment Models. Acetyl phosphate (AcP), methyl phosphate (MP) and *p*-tolyl phosphate (TP) were studied in their dianionic form interacting with either hydrogen fluoride (HF) or water (H_2O). Three different interactions (four for AcP) between the phosphorylated molecules and one molecule of HF were considered, see Figure 2. The first interaction studied was between the terminal oxygens of the phosphate, denoted by O_T, and the hydrogen of HF; here written as O_T···HF. The second was the interaction between the bridging oxygen of the phosphate, O_B, and the hydrogen of HF; here written as O_B···HF. The third was the interaction between the phosphorus and the fluorine atom of HF; here written as P···FH. This interaction was modeled in order to study the effect of the surrounding Lewis bases; the closest interaction was

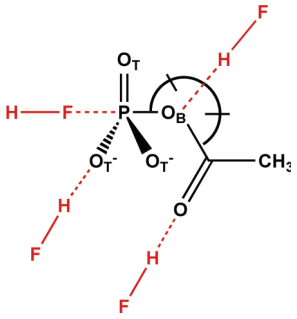

Figure 2. Positioning of HF molecules relative to AcP. The HFs involved in the O_T···HF, P···FH, and C═O···HF interactions were fixed at several distances in line with the adjacent P−O_T, P−O_B, and C═O bonds. For O_B···HF, the HF was placed at fixed distances from O_B on the distal side of C−O_B−P. The C−O_B···HF angles were fixed to a value of approximately half the value of the C−O_B−P angle.

constrained down to 2.3 Å, which is shorter than the sum of the van der Waals radii of P and F (3.27 Å)[44] but longer than a P−F single bond. For AcP the interaction between the carbonyl oxygen, (C═)O, and the HF was also studied; here written as C═O···HF. For all interactions, HF was positioned at different fixed distances from the O_T, P, and (C═)O atoms and in line with the adjacent P−O_T, P−O_B, and C═O bonds for the O_T···HF, P···FH, and C═O···HF interactions, respectively (see Table S1 in the Supporting Information). For O_B···HF, HF was placed at fixed distances from O_B and on the distal side of the C−O_B−P fragment. The C−O_B···HF angles were fixed to a value of approximately half the value of the C−O_B−P angle. For all calculations, the H−F bond length was fixed to 0.94 Å. This constraint is an approximate measure to preserve the properties of the HF molecules. For all the calculations including only one HF molecule, we used $\varepsilon = 78.39$.

Models where AcP, TP, and MP interact with three to seven HF or H_2O molecules were constructed in a similar way as for one HF. The dielectric constants used and the constrained distances between the interacting and phosphorylated molecules are given in Table S1 in the Supporting Information. If nothing else is stated in the table, no angles or H−F bond distances were constrained. For a few of the models, there were no constraints at all. All the optimized geometries were analyzed using the ChemCraft program[37] and the XYZ-viewer program.[38]

2.2. Protein Environment Models. Two models were constructed to describe the active site of Ca^{2+}-ATPase. These were constructed from the crystal structures (PDB: 2ZBF[24] and 1WPG[39]) of the E2P analogues obtained with BeF_3^- and MgF_4^{2-}. In these crystal structures, the BeF_3^- analogue models the reactant of the dephosphorylation reaction, while the MgF_4^{2-} analogue models the product state after the hydrolysis. A major difference between the two structures is the positioning of the TGES-loop: in the MgF_4^{2-} analogue, Glu183 is pointing into the active site and thereby positioning a water molecule close to the phosphorylated Asp351 so that hydrolysis can occur.[40] We will call the model derived from this structure the active model. In the BeF_3^- analogue, Glu183 is pointing away from the active site, and in this structure, the space around the BeF_3^- molecule is very compact leaving no space for an attacking water molecule. We will refer to this as the inactive model.

The quantum chemistry cluster approach was used when constructing the models.[35] The aim is to use quantum chemistry on a relatively small, well-chosen fragment of the enzyme, which represents the enzyme and ideally reacts like the real system.

dx.doi.org/10.1021/jp206414d | J. Phys. Chem. B 2012, 116, 2751−2757

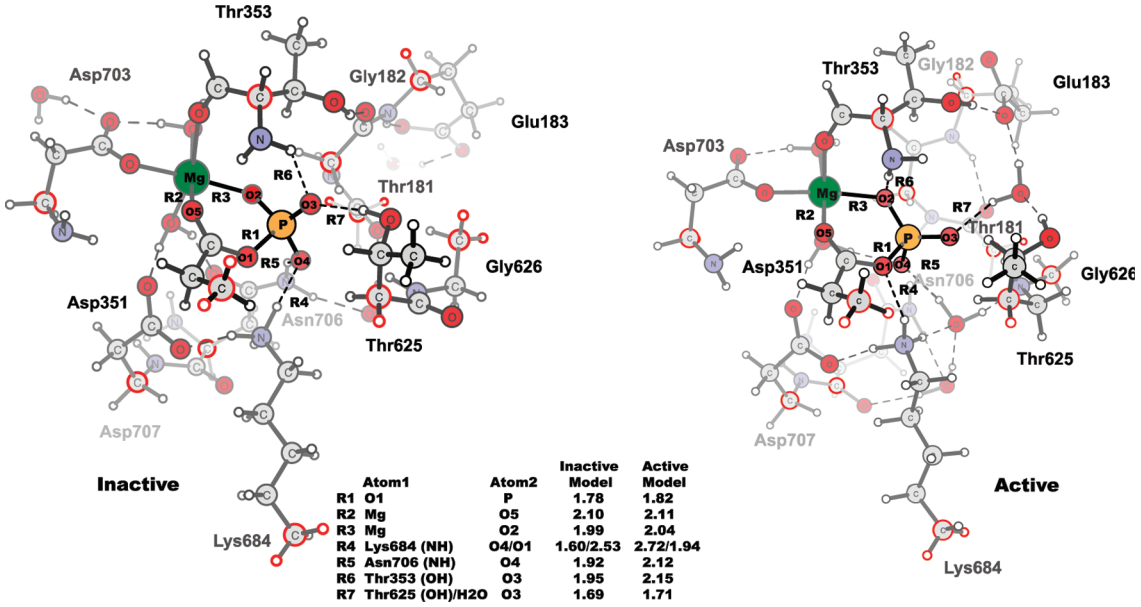

Figure 3. Optimized structure for the catalytic site of E2P using the PDB structures 2ZBF (inactive) and 1WPG (active) as starting geometries. The atoms encircled in red are those that were frozen to the crystal structure coordinates. The distances R1−R6 are given in the table in Ångströms.

Asp351 bound to phosphate (see Figure 3), a magnesium ion, five H_2O molecules (two of which are ligated to Mg), and the following amino acids, Thr181, Gly182, Glu183, Thr353, Thr625, Gly626, Lys684, Asp703, Asn706, and Asp707, were all extracted from the PDB file. To further reduce the model size, the residues were truncated so that only the side chains and backbone atoms involved in interactions with other model atoms were included. The backbone carbon and nitrogen atoms were substituted by hydrogen atoms and fixed to the crystal structure coordinates along with the α-carbon (see red encircled atoms in Figure 3). The purpose of fixation of the atoms is to keep the backbone positioned and to prevent unnatural movements, thus keeping the computational model structure close to the experimental structure during geometry optimizations.[41] The hydrogen atoms were added manually, and the side chains of glutamate, aspartate, and lysine were all charged, which is in accordance with the physiological pH 7.4. The total charge of both systems was −2, which is the charge of the phosphate substrate.

2.3. Density Functional Theory Calculations. All calculations were performed with the Gaussian03 program.[25] Geometries were optimized with a few constraints, depending on the model (see Table S1 in the Supporting Information), using density functional theory (DFT) with the B3LYP functional[26,27] and the 6-31++G(d,p) basis set:[28,29] a double-ζ basis set with both polarization and diffuse functions for all atoms. The basis set was chosen based on previous studies of Rudbeck et al.[30,31] that have shown that the geometries of phosphorylated geometries are well described with this basis set. For all geometry optimizations, solvent effects were taken into account using a self-consistent polarization model (PCM). More specifically, the conductor-like screening model (CPCM)[32,33] with settings for water (ε = 78.39) or a protein environment model (ε = 4[34,35]) was chosen.

The charges and the natural bond orbitals (NBO) were calculated for the optimized geometries using NBO 3.1[13] implemented in Gaussian03. The stabilization energy due to donor−acceptor interactions (delocalization) in negative hyperconjugation, E(2), estimates the strength of the donor−acceptor interaction and is given by eq 1.

$$E(2) = n_{\text{donor}} \frac{F_{ij}^{\,2}}{\Delta E} \tag{1}$$

F_{ij} is the Fock matrix element between orbital i and j, describing the overlap between the two orbitals. ΔE is the energy gap between the two orbitals and n_{donor} the occupancy of the lone pair. The B3LYP functional overestimates E(2),[36] and we therefore only consider relative changes between different structural models. For some of the calculations on TP, the NBO analysis did not suggest the σ(P−O_B) bond as part of the best Lewis structure. For a few selected models, we therefore suggest an alternative Lewis structure (see Figure S3 in the Supporting Information). Since the charge is unaffected by the choice of Lewis structure, it was calculated for all models.

3. RESULTS AND DISCUSSION

This section is divided into four subsections, all of which deal with different properties of the phosphate dianions. The structure and relative energies subsection describes how the P−O_B bond length and the relative energies are affected by the HF and H_2O interactions. The charge and the angle subsections show how the interactions affect the charge of the molecules and the angles of the phosphate moiety. The negative hyperconjugation section describes how this effect stabilizes or destabilizes the P−O_B bond.

3.1. Structure and Relative Energies. The effect of individual interactions on the length of the scissile P−O bond is of strong interest since an elongation of this bond is related to a decrease in activation energy and thus a rate enhancement.[11] The four interactions O_B···HF, O_T···HF, C═O···HF, and P···FH were studied here to determine their effect in weakening the P−O_B bond. As mentioned in the Introduction, the reason to use HF instead of H_2O is to study single interactions, which is difficult with H_2O as a computational model since water energetically prefers to hydrogen bond to more than one oxygen. Figure 4 shows the relationship between the P−O_B

dx.doi.org/10.1021/jp206414d | J. Phys. Chem. B 2012, 116, 2751−2757

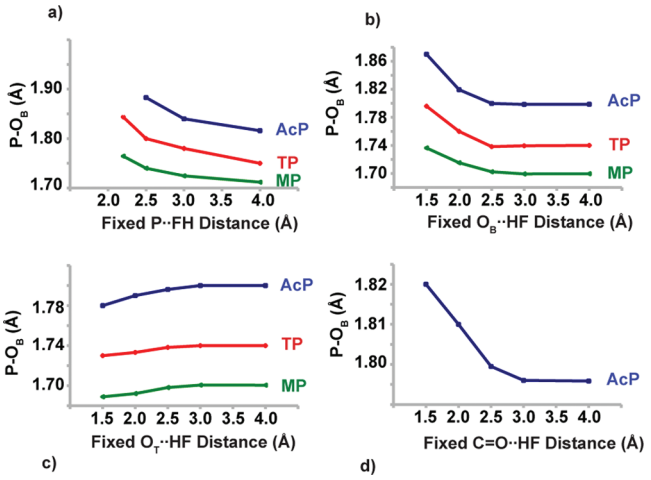

Figure 4. P−O_B bond length change for different HF interactions: a, P···FH; b, O_B···HF; c, O_T···HF; d, C═O···HF (the interactions are shown in Figure 2). Blue is AcP, red is TP, and green is MP.

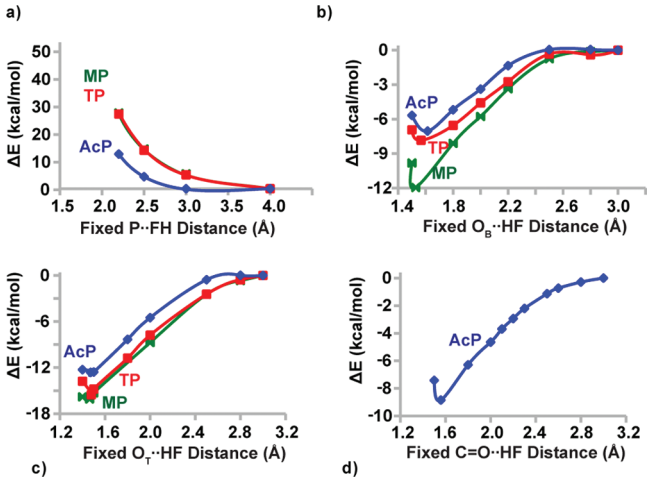

Figure 5. Relative energy (geometry optimized energy at given distance minus the energy at the longest distance) of the HF interactions: a, P···FH; b, O_B···HF; c, O_T···HF; d, C═O···HF. Blue is AcP, red is TP, and green is MP. The O···H distance in panels b−d is not constrained for the points with the lowest energy.

bond length and the fixed distance between HF and the different phosphorylated molecules.

Strong O_B···HF interactions increase the P−O_B distance for all molecules significantly (∼0.05 Å); however, the O_B···HF interaction alone is too weak to break the bond, even at a constrained distance of 1.5 Å. The bond elongation effect is largest for AcP (∼0.08 Å for an HF approach from 4 to 1.5 Å), intermediate for TP (∼0.06 Å), and smallest for MP (∼0.04 Å). The corresponding weakening, in terms of bond valence,[42,43] is ∼15% for AcP and TP and ∼10% for MP. For AcP, the P−O_B bond length also increases when decreasing the C═O···HF distance, the effect is however not as strong (<0.03 Å), and the bond weakens by 6%. In contrast, the O_T···HF interaction strengthens the P−O_B bond, and this will result in a less reactive compound, in line with the solvent study by DeMeis and Vianna.[7] The largest bond length change is again observed for AcP (−0.02 Å for an HF approach from 4 to 1.5 Å), while that observed for TP and MP is smaller (−0.01 Å) corresponding to a strengthening by ∼5% for AcP and 3% for TP and MP. The effect of short P···FH interactions, i.e., less than the sum of van der Waals radii of P and F, on the P−O_B bond lengthening in the three models is found strongest for AcP compared to TP and MP (Figure 4).

Figure 5 shows the distance dependence of the relative energies (geometry optimized energy at given distance minus the energy at the weakest interaction) for the different interactions. When the fluorine atom of the HF molecule approaches the phosphorus, the relative energy increases for all three molecules and thereby has a destabilizing effect (Figure 5). This figure shows that between the three amino acid models, the surrounding Lewis bases have a higher energetic effect on MP and TP compared to AcP. When the hydrogen of the HF molecule approaches the oxygens and forms hydrogen bonds, the energy for all three phosphorylated molecules decreases, as expected. The favorable effects are smallest for interactions to the O_B and O_T atoms of AcP, but this molecule has an extra site (C═O) for hydrogen bonding compared to MP and TP. The sum of van der Waals radii of oxygen and hydrogen is in total 2.7 Å (1.2 Å for hydrogen and 1.52 Å for oxygen),[44] where the relative energy converges to zero and thus no longer is affected by the hydrogen bond (see Figure 5). The calculations show that the P−O_B bond of AcP is most susceptible to bond deformation by external interactions, whereas MP is least affected. Of the four interactions studied, O_B···HF (or H_2O) and C═O···HF (or H_2O) are the only interactions that both weaken the P−O_B bond and energetically stabilize the system.

The interaction effects were also studied for the protein models. The P−O_B bond length in the inactive model (1.78 Å) is shorter compared to that of the active structure (1.82 Å). One noticeable explanation for this elongation is the hydrogen bond between the Lys684 and the phosphorylated Asp351 (see Figure 3 and Table 1). In the inactive model, the lysine forms a linear hydrogen bond to one of the phosphate's terminal oxygens, while in the active structure, it hydrogen bonds to the bridging oxygen. Our results in Figure 4 show that a P−O_B bond distance is shorter if an interacting molecule hydrogen bonds to the phosphate molecule's terminal oxygens compared to a hydrogen bond to the bridging oxygen, which explains the elongation in the active structure of the protein.

Table 1. Distances in Å between Several Heavy Atoms in the Protein Models and in the Crystal Structure[a]

			inactive		active	
	atom1	atom2	model	crystal	model	crystal
R1	O1	P	1.78	1.6	1.82	2.5
R2	Mg	O5	2.1	2.2	2.11	2.2
R3	Mg	O2	1.99	1.9	2.04	2
R4	Lys684 (N)	O4/O1	2.67/2.72	2.9/3.0	3.27/2.79	4.6/3.7
R5	Asn706 (N)	O4	2.86	3.1	2.99	3
R6	Thr353 (O)	O3	2.94	2.9	3.16	2.9
R7	Thr625 (O)/H_2O	O3	2.66	2.6	2.76	2.5

[a]R1−R7 are defined in Figure 3.

3.2. Charge Effect. Electrostatic interactions are due to the nonuniform distribution of positive and negative charges. In a protein, these interactions reflect a preorganized polar environment of the enzyme's active site.[45] In the following section, we describe charge changes induced by the interactions between HF/H_2O and the phosphorylated molecules and thereby show

dx.doi.org/10.1021/jp206414d | J. Phys. Chem. B 2012, 116, 2751−2757

how an environment can stabilize the dianionic phosphate group through electrostatic interactions.

There are two ways for the dianionic phosphate group to delocalize its charge: either it can transfer some of the charge to the interacting molecules or the P−O_B bond can be elongated and thereby transfer charge to O_B. We studied the charge of the phosphate molecule, of the interacting molecules, and of the whole organic group (O_B−R), i.e., subtracting the charge of the phosphate group and the interacting molecules from the total charge of the model. Since the charge of the O_B atom can be delocalized to the organic group that it is bonded to, it is more appropriate to study the charge of the O_B−R group compared to the charge of only the O_B atom.

First, the charge effect of single interactions was studied (Figure 6), between the three phosphorylated molecules and

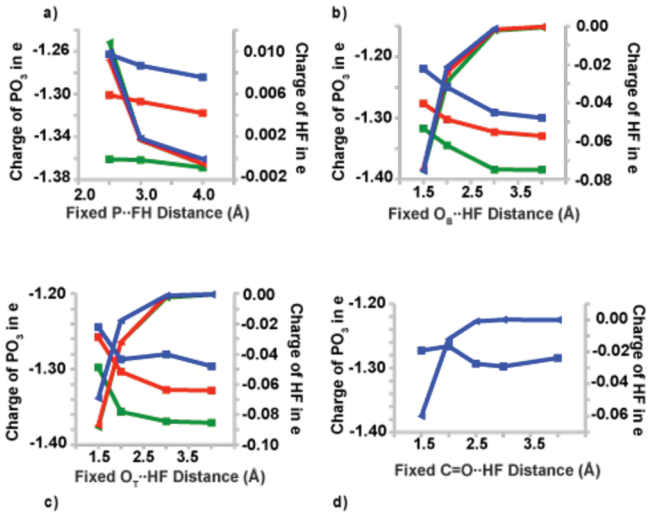

Figure 6. Charge of the P(O_T)$_3$ moiety (squares) and the HF molecule (triangle) when the phosphorylated molecules interact with one HF molecule: a, P···FH; b, O_B···HF; c, O_T···HF; d, C═O···HF. Blue is AcP, red is TP, and green is MP.

one HF molecule. For all the models with a hydrogen bond interaction (O···H), the charge of the HF molecule decreases and becomes more negatively charged, when the O···H distance is shortened. For all interactions, the negative charge of the phosphate group decreases, when the interacting molecule approaches.

For the organic group, the effect of the interactions differs, stronger O_T···H interaction leads to a less negative charge since the P−O_B bond is shortened. During an approach of the HF to the O_B atom, the charge increases (more negative), which is explained by a longer P−O_B bond. That the charge of the organic group is primarily affected by the P−O_B bond length, and not from charge transfer between the organic group and the interacting molecules, is shown in Figure 7. In the figure, a correlation can be observed between the charge of the organic group and the P−O_B bond length

In the Ca^{2+}-ATPase, the H-bond from the NH_3 group of Lys684 shifts from interacting with O_T in the inactive model to O_B in the active model. From our simple models, we see that such a shift would contribute to a more negatively charged O_B atom and a longer P−O_B bond. In agreement, the P−O_B bond of the active model is 0.04 Å longer, and the charge of the O_B atom is 0.03e lower compared to the inactive model.

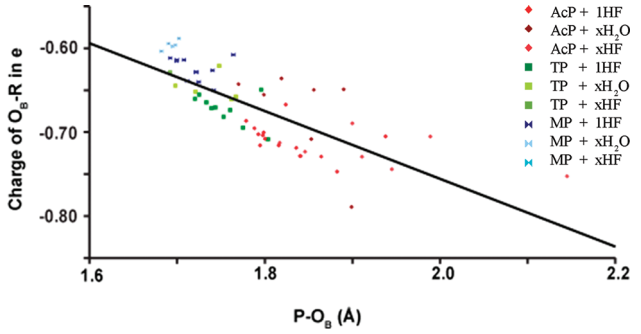

Figure 7. Correlation between the P−O_B bond length and the charge sum of the O_B−R moiety for the phosphorylated molecules interacting with HF or H_2O molecule(s). The legend on the right defines the different colors (x = 3−7). The charge of the protein models is not included in the figure.

3.3. Angle Effect. Since it is easier for an attacking nucleophile to approach a more widened phosphate group, the bond angles in the phosphorylated amino acids are important descriptors.[17] In this section, we will therefore explore whether interactions with the environment affect bond angles and whether bond angle effects are correlated to the P−O_B bond length.

Figure 8 includes all interactions between the three phosphorylated molecules and the HF/H_2O molecule(s) and the protein models. In the absence of the interactions, the average O_TPO_T angle is 116° for AcP, 115° for TP, and 113° for MP, and the average O_TPO_B angle is 103° for AcP, 104° for TP, and 106° for MP. In other words, the phosphate group in AcP seems to be the most exposed to a potential nucleophile, although the differences are small. For the models with interactions, the most narrow O_TPO_B angle modeled is for AcP with an angle of 95°, the same model has an O_TPO_T angle of 119°, a value that is close to those expected for both loose and tight transition states in dephosphorylation reactions.[46] This shows that some of our models reflect transition state properties, although the calculations shown here are not transition state optimized. Figure 8 demonstrates that there is a linear correlation between the P−O_B bond length and the average O_TPO_T (R^2 = 0.76) and O_TPO_B (R^2 = 0.79) angles. Lager and Gibbs[47] and Brown and Gibbs[48] have earlier been presented a similar linear correlation. They studied phosphates with different substituents, while our study deals with environmental effects. We conclude that intra- and intermolecular effects that lengthen the P−O_B bond also widen the O_TPO_T angle and narrow the O_TPO_B angle.

In the Ca^{2+}-ATPase models, the aspartyl phosphate's C═O, O_T, and O_B atoms all either interact with Mg^{2+} or are hydrogen bonded to different amino acids. The difference to the simpler models is that the phosphate angles in the Ca^{2+}-ATPase diverge more due to a more asymmetric environment with different types of interactions. However, the averages of the O_T−P−O_B and O_TPO_T angles (102°/116° for the active model and 103°/115° for the inactive model) at least follow the trend of AcP, MP, and TP interacting with the HF and H_2O molecules.

3.4. Negative Hyperconjugation. A weak P−O_B bond can be explained by negative hyperconjugation where the $n(O_T)$ orbitals donate electrons to the antiperiplanar σ^*(P−O_B) orbital (see Figure 9). We studied the extent of the negative hyperconjugation, when HF and H_2O interact with AcP, MP, and TP by performing natural bond orbital (NBO) analysis. From the literature, it is known that methylation or protonation of a phosphate distorts the antiperiplanar lone pair, meaning that the

dx.doi.org/10.1021/jp206414d | J. Phys. Chem. B 2012, 116, 2751−2757

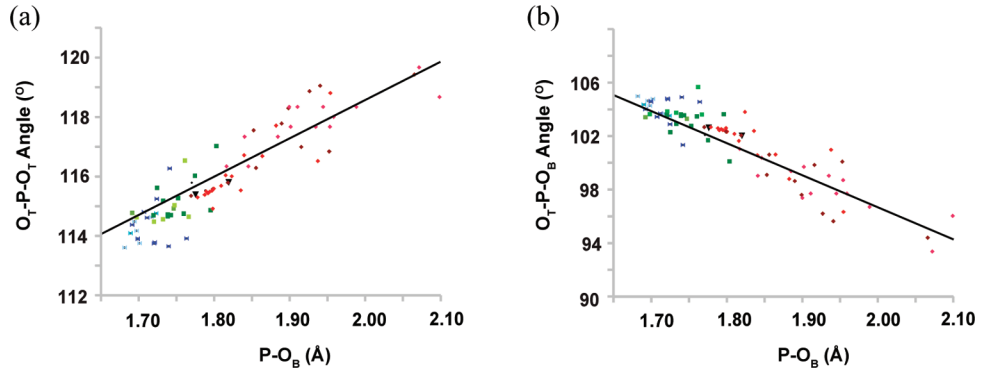

Figure 8. Linear correlation between P−O_B bond distance and (a) the O_TPO_B bond angle (R^2 = 0.76) and (b) O_TPO_T bond angle (R^2 = 0.79). See Figure 7 for the different color definitions (black triangles = the inactive/active protein models).

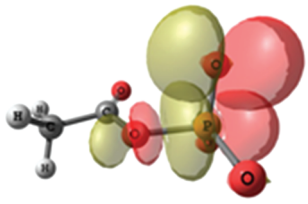

Figure 9. Natural bond orbitals of σ^*(P−O_B) and n(O_T). The figure shows the overlap between the two orbitals.

overlap between the O_T lone pair orbital and the σ^*(P−O_B) orbital is reduced.[6,8,9,12,49] Before including interacting HF or H_2O molecule(s), the phosphates were therefore examined whether different molecular geometries can introduce an orbital overlap reduction. This test was performed in order to avoid that the energy minimized structures exhibit extraordinary negative hyperconjugation. Only minor effects were found (see Table S2 in the Supporting Information).

The E(2) energy was calculated for all interactions except for TP interacting with more than one HF or H_2O molecule due to the complications of finding appropriate Lewis structures (see Supporting Information). The correlation between the P−O_B bond distance and E(2) shows that the bond distance increases linearly with the stabilization energy, see Figure 10 (R^2 = 0.93).

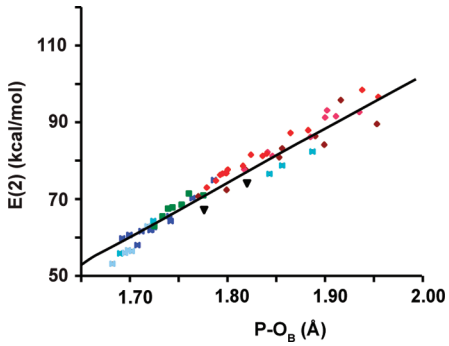

Figure 10. Linear correlation (R^2 = 0.93) between the stabilizing energy, E(2), and the P−O_B bond distance. See Figure 7 for the different color definitions definitions (black triangles = the inactive/active protein models).

The energy difference of E(2) between calculations performed with HF/H_2O at short (2−2.5 Å) and longer (4 Å) distances varies between 4 and 20 kcal/mol (17 and 84 kJ/mol) depending on the interaction and the molecule.

Concomitant with a stronger negative hyperconjugation at longer P−O_B bond lengths, the occupancy of the σ^*(P−O_B)-orbital increases, as shown in Figure S5 in the Supporting Information. The donor orbitals, the O_T n-orbitals, are located on the phosphate group, while the σ^*(P−O_B)-orbital is partly located on a leaving group atom. Therefore, its higher occupancy readily explains the charge transfer to the leaving group upon bond elongation.

4. CONCLUSIONS

Enzymes use precisely controlled interactions for catalysis. In order to explore the role of individual interactions on phosphorylated amino acids and their implications for the dephosphorylation reaction, the model substances MP, TP, and AcP were studied interacting with hydrogen fluoride and water. While an O_T···HF interaction strengthens the P−O_B bond (Figure 4), a strong hydrogen bond interaction to the bridging oxygen O_B elongates the P−O_B bond (Figure 4) and widens the O_TPO_T angle (Figure 8). Such a flattening of the phosphate thereby exploits the phosphorylated amino acids for a nucleophilic attack.[17] For AcP, a hydrogen-bond interaction to the C═O group causes the same trends as the same type of interaction to O_B but to a smaller extent.

The three studied molecules exhibit different sensitivities on a given interaction. In terms of P−O_B bond length and strength, AcP is the most effected, whereas MP is the least affected. TP has intermediate sensitivity for the bond elongating interactions but resembles MP for the bond shortening interaction to O_T. AcP is also most susceptible on a given interaction to the widening of the O_TPO_T angle of the three model molecules; the phosphate group of AcP is thereby most easily exposed to a nucleophile attack.

An enzyme may use the interactions to the organic group of the substrate to destabilize the P−O_B bond and to strain the reactant in the ground state. The binding energy of these favorable interactions can be used to partly compensate an unfavorable weakening of interactions to the O_T atoms, which will also destabilize the P−O_B bond. A further strengthening of the interactions with the organic group can help to reduce the energy penalty of the approach of the attacking nucleophile. These interactions stabilize also the negative charge that develops on the organic group when the P−O_B bond elongates. Thus, stronger interactions with the organic group and weaker interactions with the phosphate O_T atoms make the phosphorylated amino acids more product-like in terms of structure and charge distribution. In this way, an enzyme can fine-tune its interactions in order to

dx.doi.org/10.1021/jp206414d | J. Phys. Chem. B 2012, 116, 2751−2757

adjust the activation energy of dephosphorylation according to the rate required for its function.

That our simple environmental models bear relevance also for the catalytic site of proteins was demonstrated by our models of the Ca^{2+}-ATPase in the E2P state as the protein models follow the same trends as the models with the HF and H_2O environments. In particular, in the inactive protein model, the NH_3 group of Lys684 hydrogen bonds to an O_T atom and thereby shortens the P−O_B bond, while in the inactive model, it hydrogen bonds to the O_B atom and elongates the bond. The change in interaction explains the 0.04 Å P−O_B bond length increase in the active model compared to the inactive model. Because of the elongation of the bond, the O_TPO_T angle is also slightly increased, facilitating an approach of an attacking water molecule.

■ ASSOCIATED CONTENT

Supporting Information

Table of constrained distances for the different models, a plot of the charge of the $P(O_T)_3$ moiety of all the models, and detailed information about the negative hyperconjugation including a plot of the linear correlation between the occupancy and the P−O_B bond distance. This material is available free of charge via the Internet at http://pubs.acs.org.

■ AUTHOR INFORMATION

Corresponding Author

*E-mail: maria.rudbeck@dbb.su.se (M.E.R.); andreas.barth@dbb.su.se (A.B.).

Notes

The authors declare no competing financial interest.

■ ACKNOWLEDGMENTS

We are grateful to Vetenskapsrådet for the support of this work. S.O.N.L. acknowledges The Åke Wiberg Foundation. We would also like to thank Professor M. R. A. Blomberg for valuable discussions.

■ REFERENCES

(1) Cleland, W.; Hengge, A. *Chem. Rev.* **2006**, *106*, 3252−3278.
(2) Bruice, T. C. *Chem. Rev.* **2006**, *106*, 3119−3139.
(3) Hur, S.; Bruice, T. *J. Am. Chem. Soc.* **2003**, *125*, 1472−1473.
(4) Cheng, H.; Sukal, S.; Deng, H.; Leyh, T.; Callender, R. *Biochemistry* **2001**, *40*, 4035−4043.
(5) Ruben, E.; Chapman, M.; Evanseck, J. *J. Phys. Chem. A* **2007**, *111*, 10804−10814.
(6) Ruben, E.; Plumley, J.; Chapman, M.; Evanseck, J. *J. Am. Chem. Soc.* **2008**, *130*, 3349−3358.
(7) DuPre, D. B.; Vorobyov, I.; Yappert, M. C. *J. Mol. Struct.* **2001**, *544*, 91−109.
(8) Gorenstein, D.; Luxon, B.; Findlay, J. *J. Am. Chem. Soc.* **1977**, *99*, 8048−8049.
(9) Range, K.; McGrath, M.; Lopez, X.; York, D. *J. Am. Chem. Soc.* **2004**, *126*, 1654−1665.
(10) Lad, C.; Williams, N.; Wolfenden, R. *Proc. Natl. Acad. Sci. U.S.A.* **2003**, *100*, 5607−5610.
(11) Jones, P.; Kirby, A. *J. Am. Chem. Soc.* **1984**, *106*, 6207−6212.
(12) Denehy, E.; White, J.; Williams, S. *Inorg. Chem.* **2007**, *46*, 8871−8886.
(13) Glendening, J. E.; Badenhoop, K.; Reed, A.; Carpenter, J.; Bohmann, J.; Morales, C.; Weinhold, F. *NBO 3.1 Program*; Theoretical Chemistry Institute, University of Wisconsin: Madison, WI, 1990.
(14) Abell, K.; Kirby, A. *Tetrahedron Lett.* **1986**, *27*, 1085−1088.
(15) Grzyska, P.; Czyryca, P.; Golightly, J.; Small, K.; Larsen, P.; Hoff, R.; Hengge, A. *J. Org. Chem.* **2002**, *67*, 1214−1220.
(16) de Meis, L.; Suzano, V. *FEBS Lett.* **1988**, *232*, 73−77.
(17) Barth, A.; Bezlyepkina, N. *J. Biol. Chem.* **2004**, *279*, 51888−51896.
(18) Klähn, M.; Schlitter, J.; Gerwert, K. *Biophys. J.* **2005**, *88*, 3829−3844.
(19) Wang, J. H.; Xiao, D. G.; Deng, H.; Webb, M.; Callender, R. *Biochemistry* **1998**, *37*, 11106−11116.
(20) Allin, C.; Gerwert, K. *Biochemistry* **2001**, *40*, 3037−3046.
(21) Belasco, J. G.; Knowles, J. R. *Biochemistry* **1980**, *19*, 472−477.
(22) Wharton, C. W. *Nat. Prod. Rep.* **2000**, *17*, 447−453.
(23) Barth, A.; Krasteva, M. *Biochim. Biophys. Acta* **2007**, *1767*, 114−123.
(24) Toyoshima, C.; Norimatsu, Y.; Iwasawa, S.; Tsuda, T.; Ogawa, H. *Proc. Natl. Acad. Sci. U.S.A.* **2007**, *104*, 19831−19836.
(25) Frisch, M. J.; Trucks, G. W.; Schlegel, H. B.; Scuseria, G. E.; Robb, M. A.; Cheeseman, J. R.; Montgomery, J. A., Jr.; Vreven, T.; Kudin, K. N.; Burant, J. C.; Millam, J. M.; Iyengar, S. S.; Tomasi, J.; Barone, V.; Mennucci, B.; Cossi, M.; Scalmani, G.; Rega, N.; Petersson, G. A.; Nakatsuji, H.; Hada, M.; Ehara, M.; Toyota, K.; Fukuda, R.; Hasegawa, J.; Ishida, M.; Nakajima, T.; Honda, Y.; Kitao, O.; Nakai, H.; Klene, M.; Li, X.; Knox, J. E.; Hratchian, H. P.; Cross, J. B.; Bakken, V.; Adamo, C.; Jaramillo, J.; Gomperts, R.; Stratmann, R. E.; Yazyev, O.; Austin, A. J.; Cammi, R.; Pomelli, C.; Ochterski, J. W.; Ayala, P. Y.; Morokuma, K.; Voth, G. A.; Salvador, P.; Dannenberg, J. J.; Zakrzewski, V. G.; Dapprich, S.; Daniels, A. D.; Strain, M. C.; Farkas, O.; Malick, D. K.; Rabuck, A. D.; Raghavachari, K.; Foresman, J. B.; Ortiz, J. V.; Cui, Q.; Baboul, A. G.; Clifford, S.; Cioslowski, J.; Stefanov, B. B.; Liu, G.; Liashenko, A.; Piskorz, P.; Komaromi, I.; Martin, R. L.; Fox, D. J.; Keith, T.; Al-Laham, M. A.; Peng, C. Y.; Nanayakkara, A.; Challacombe, M.; Gill, P. M. W.; Johnson, B.; Chen, W.; Wong, M. W.; Gonzalez, C.; Pople, J. A. *Gaussian 03*, revision D.01; Gaussian, Inc.: Wallingford, CT, 2003.
(26) Becke, A. *J. Chem. Phys.* **1993**, *98*, 5648−5652.
(27) Lee, C.; Yang, W.; Parr, R. *Phys. Rev. B* **1988**, *37*, 785−789.
(28) Francl, M.; Pietro, W.; Hehre, W.; Binkley, S.; Gordon, M.; DeFrees, D.; Pople, J. *J. Chem. Phys.* **1982**, *77*, 3654−3665.
(29) Hehre, W. J.; Ditchfield, R.; Pople, J. A. *J. Chem. Phys.* **1972**, *56*, 2257−2261.
(30) Rudbeck, M. E.; Kumar, S.; Mroginski, M. A.; Nilsson Lill, S. O.; Blomberg, M. R. A.; Barth, A. *J. Phys. Chem. A* **2009**, *113*, 2935−2942.
(31) Rudbeck, M. E. *Int. J. Quantum Chem.* **2011**, DOI 10.1002/qua.23182.
(32) Barone, V.; Cossi, M. *J. Phys. Chem. A* **1998**, *102*, 1995−2001.
(33) Cossi, M.; Rega, N.; Scalmani, G.; Barone, V. *J. Comput. Chem.* **2003**, *24*, 669−681.
(34) Noodleman, L.; Lovell, T.; Han, W.-G.; Li, J.; Himo, F. *Chem. Rev.* **2004**, *104*, 459−508.
(35) Siegbahn, P. E. M.; Himo, F.; Wiley. Interdisciplinary Reviews: Computational Molecular. *Science* **2011**, *1*, 323−336.
(36) Nilsson Lill, S. O.; Rauhut, G.; Anders, E. *Chem. Eur. J* **2003**, *9*, 3143−3153.
(37) Zhurko, G. A.; Zhurko, D. A. *ChemCraft Program*, version 1.6, build 315; 2009. www.chemcraftprog.com.
(38) de Marothy, S. A. *XYZViewer*, version 0.963; 2011. http://www.physto.se/~sven.
(39) Toyoshima, C.; Nomura, H.; Tsuda, T. *Nature* **2004**, *432*, 361−368.
(40) Olesen, C.; Sørensen, T. L.-M.; Nielsen, R. C.; Møller, J. V.; Nissen, P. *Science* **2004**, *306*, 2251−2255.
(41) Siegbahn, P. E. M. *J. Comput. Chem.* **2001**, *22*, 1634−1645.
(42) Brown, I. D. *The Chemical Bond in Inorganic Chemistry: The Bond Valence Model*; Oxford University Press: Oxford, U.K., 2002.
(43) Brown, I.; Wu, K. *Acta Crystallogr., Sect. B: Struct. Sci.* **1976**, *32*, 1957−1959.
(44) Bondi, A. *J. Phys. Chem.* **1964**, *68*, 441−451.
(45) Warshel, A. *J. Biol. Chem.* **1998**, *273*, 27035−27038.
(46) Mildvan, A. S. *Proteins* **1997**, *29*, 401−416.
(47) Lager, G.; Gibbs, G. V. *Am. Mineral.* **1973**, *58*, 756−764.
(48) Brown, G.; Gibbs, G. *Am. Mineral.* **1970**, *53*, 1587−1607.
(49) Gorenstein, D.; Luxon, B.; Findlay, J.; Momii, R. *J. Am. Chem. Soc.* **1977**, *99*, 4170−4172.